Analyst

PAPER

View Article Online
View Journal | View Issue

Cite this: *Analyst*, 2014, **139**, 1492

Dynamics of BSA adsorption onto a photoablated polymer surface in a dielectric microchip

Mohammed kechadi,[abc] Lila Chaal,[c] Bernard Tribollet[ab] and Jean Gamby*[ab]

Received 4th November 2013
Accepted 2nd January 2014

DOI: 10.1039/c3an02068a

www.rsc.org/analyst

Dielectric impedance spectroscopy in a microchip was used for monitoring the adsorption of biomolecules onto a heterogeneous polymer surface obtained after the photoablation process. The sensor comprises a thin dielectric layer with two parallel carbon microband electrodes on the one side, and the photoablated surface on the other. The biomolecules need not to be labelled, as in an optical biosensor, even if they need to be attached to the polymer surface coupled with the microelectrodes when a biomolecular interaction occurs. Based on this principle, a flow sensor has been developed to record the adsorption dynamics illustrated with BSA coating on the heterogeneous surface in a linear dynamic range from 1 picomolar to 1 nanomolar at a fixed low frequency. Modeling the dielectric interface using an appropriate equivalent circuit permits extraction of the values of the interfacial impedance for ultralow protein concentrations. The promising results obtained with this methodology make it a competing method in comparison with optical or electrochemical transduction for biosensor development.

1 Introduction

Direct immunosensors can detect interactions between ligands by measuring changes in capacitance,[1,2] mass,[3,4] or fluorescence.[5,6] Optical biosensors measure the variation in the intrinsic optical properties of a surface onto which a dielectric material is loaded.[7,8] They are widely used and allow obtaining dynamic interaction data between ligands. One of the most used instruments is one that takes advantage of surface plasmon resonance (SPR).[9] For this, the metal/dielectric interface is excited by a beam of monochromatic light, under the conditions of total reflection leading to the famous resonance. The intensity of the reflected light at a specific angle has a depth in which the intensity is operable. Several factors influence the position of the resonance angle, which is a refractive index of the medium close to the face of the non-excited metallic thin film. The concentration of dissolved species is thus determined in the medium as it is directly related to the refractive index.[9,10]

As is shown, a conventional SPR cell biosensor has two parts: the channel flow and the region in which the interactions between ligands take place. The ligand is immobilized on the sensor surface while the analyte continuously flows over the entire surface.

The main advantage of the SPR methodology is to detect label-free and real-time processes of association and dissociation of ligands. However, its disadvantage is the absolute necessity to immobilize the ligand to drastically increase the amount of analyte bound. This has resulted in a successful research development in surface chemistry functionalization to immobilize ligands, such as antibodies, in a functional and controlled orientation in order to increase the sensitivity of SPR immunoassays. Detection of the recognition elements on the SPR sensor is performed using intermediate chains such as alkanethiols, silanes, or polypeptides grafted on the sensor surface. However, the use of a soft hydrogel matrix composed of carboxylmethylated dextran chains remains the most common strategy. The porous three-dimensional matrix hydrogel is attached to the sensor surface, which increases the length of the plasmon arising from the thin gold film (100 nm). Thus, a protein adsorbed or bound to the matrix induces a radical change in the activity of the latter. The hydrogel acts as a tertiary structure of the protein at or near the active site, where the binding of interest may be modified by the immobilization step, thereby changing its properties. The steric hindrance encountered by the analyte in the hydrogel constitutes another drawback.[11–13]

In recent years, a new kind of electrical biosensor has been developed. It is based on the capacitive coupling between microelectrodes galvanically isolated in a dielectric polymer such as polyethylene terephthalate (PET). Over the PET, a flow microchannel is fabricated by a laser photoablation procedure.[14,15] Briefly, the principle is to sandwich a thin dielectric PET layer (5 μm) between the two microelectrodes (electronic charge) and a flow microchannel (ionic charge). More recently a detailed methodology for non-contact impedance in such a dielectric microdevice has been published.[16] This method eliminates the contribution of the impedance of the thin 120 μm PET layer which separates the two embedded

[a]*CNRS, UMR 8235, Laboratoire Interface et Systèmes Electrochimiques, (LISE), F-75005 Paris, France. E-mail: jean.gamby@upmc.fr; Fax: +33 0144274074; Tel: +33 0144273640*

[b]*Sorbonne Universités, UPMC Univ Paris 06, UMR 8235, Laboratoire Interfaces et Systèmes Electrochimiques, (LISE), 4 Place Jussieu, F-75005, Paris, France*

[c]*Laboratoire d'Electrochimie, Corrosion et de Valorisation Energétique (LECVE), Faculté de Technologie, Université A. MIRA, Béjaia 06000, Algeria*

microelectrodes (see Fig. 1A). This procedure enables a clear observation of the microchannel impedance associated in series with the interfacial impedance, Z_{int}, together with the impedance of the 5 μm PET non-contact layer from the microelectrode to the microchannel bottom.

Indeed, eliminating the contribution of the impedance of the polymer between the two microelectrodes enables new applications at high frequencies.[15] This article is a direct and practical application to monitor the interfacial impedance at low frequencies where correction is not needed. The PET surface can be of various kinds, depending on the modification of the polymer. In this way the effect of the state of the surface on the activity of biomolecules can be investigated.

It will be shown here that the described methodology using dielectric measurement is more practical and less time-consuming than other techniques. In comparison to the SPR principle, the diffusion of species is not hindered since a hydrogel is not necessary. Indeed, the amount of data collected leading to a correct interpretation of the adsorption dynamic under flow conditions constitutes a paramount importance for investigating the association dynamics of ligands on a material support.

2 Materials and methods

2.1 Chemicals

The NaCl solution (10 mM) was fixed at pH 9 with solutions of NaOH and HCl. Bovine serum albumin was purchased from VWR International (96%). A 10^{-4} M stock solution was obtained after dilution in 0.01 M NaCl.

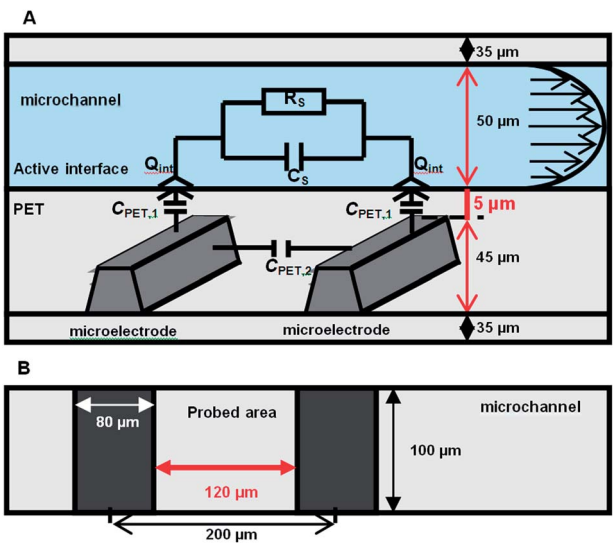

Fig. 1 (A) Representation of the microchip interfaces by an equivalent electrical circuit. $C_{PET,2}$ represents the capacitance of the 120 μm PET layer between the two parallel microelectrodes. $C_{PET,1}$ represents the impedance of the non-contact 5 μm PET layer. Q_{int} represents the interfacial impedance through the active surface. R_S and C_S represent the solution microchannel resistance and the cell capacitance, respectively. (B) Top view of the microchannel with the non-detection area.

2.2 BSA adsorption under flow conditions

Solutions of BSA with concentrations ranging from 1 pM to 500 pM in 0.01 M NaCl were pumped in a 2 cm long microchannel (50 × 100 μm in cross-section, as shown in Fig. 1B) using a syringe pump at a rate of 7.2 μL min^{-1}. The samples were adsorbed onto the photoablated PET surface and the variation in the differential impedance was recorded with time at a fixed low frequency (200 Hz).

2.3 Microchip network

The microchip device used in this work was described elsewhere.[17] Impedance measurements were carried out through a polyethylene terephthalate (PET) microchannel photoablated having a trapezoidal cross-section shape with a depth of 45 μm, a top width of 100 μm and a length of 1.4 cm. The distance separation between both microchannels is 200 μm center to center (see Fig. 1B). The electrode fabrication is achieved using a carbon ink loaded with gold nanoparticles, thermally laminated at 135 °C and a pressure of 2 bar by a polyethylene (10 μm)/polyethylene terephthalate (25 μm) (PE/PET) layer with a total thickness of 35 μm. The distance separation in the PET band between the two planar microelectrodes and the main microchannel is equal to 5 μm and the detection surface area per microelectrode is 80 μm × 100 μm.

2.4 Apparatus

Electrochemical impedance spectroscopy measurements have been performed by applying an AC voltage with constant amplitude (0.1 V) through the microelectrodes with a fixed frequency of 200 Hz. The current measured is thus related to the total impedance of the sensor. These measurements are performed using a frequency response analyzer (FRA 1255B, Solartron U.K.) together with a dielectric interface 1296 (Solartron, U.K.) which extends the frequency range from 1 Hz to 10 MHz. Data are obtained using the company-made software SMaRT. To analyze these results, a physical model is used as described in Fig. 1A.

3 Results and discussion

3.1 Methodology for realtime adsorption in the microchannel

The characteristics of this kind of interface with an insulating layer sandwiched between two galvanic isolated microelectrodes can be represented by a dielectric system with, on one part of the thin polymer layer, electronic charge on microelectrodes and, on the other part, ionic charge in the microchannel. An electrical equivalent circuit can be drafted, considering impedances for each part of the microdevice as displayed in Fig. 1A. The global impedance, Z_G, through the microdevice using free contact microelectrode configuration, is given by the sum:

$$Z_G^{-1}(\omega) = Z_1^{-1}(\omega) + Z_2^{-1}(\omega) \quad (1)$$

wherein ω is the angular frequency (rad s^{-1}), defined by $\omega = 2\pi f$, where f is the frequency (Hz).

As explained in a previous paper[16,18] the electrical impedance through the microchannel/polymer interface is defined as Z_1 and the impedance between the two galvanically isolated microelectrodes as Z_2:

$$Z_1(\omega) = \frac{2}{j\omega C_{PET,1}} + \frac{2}{(j\omega)^{\alpha_{int}} Q_{int}} + \frac{R_S}{1 + j\omega C_S R_S} \quad (2)$$

$$Z_2(\omega) = \frac{1}{j\omega C_{PET,2}} \quad (3)$$

Impedances through the 5 μm PET layer or the 120 μm PET layer are defined as capacitances $C_{PET,1}$ and $C_{PET,2}$, respectively. The PET/microchannel interface behaves as a non-ideal capacitor and is defined by a constant phase element (CPE) with Q_{int} and α_{int} being the CPE and the CPE exponent, respectively. The CPE exponent α_{int} takes into account the role of the photoablated PET surface at the microchannel bottom. In previous work alpha α_{int} was found to be equal to 0.5.[16] In the microchannel, the impedance is represented by an $R_S//C_S$ circuit. The resistance, R_S, is characteristic of the electrolyte resistance and C_S is the cell capacitance.

To make a sweep in frequency and record the electrical impedance of this filled device, the experimental setup was built by connecting the microchip to a dielectric interface apparatus dedicated for insulating material (Solartron ID1296). All the experimental set-up was computer-controlled using commercial software (Smart, Solartron Analytical). A 100 mV alternating signal was applied in a 1 MHz to 20 Hz frequency range. For the following bioanalytical application at a fixed frequency, a low frequency window was preferred because the main information contained in the imaginary part of impedance is the interfacial impedance, Q_{int}.

3.2 BSA adsorption under flow conditions

In the first step, 10^{-2} M NaCl was pumped at 7.2 μL min^{-1} in the microchannel to obtain the baseline, Z_{NaCl}, for 360 s. The corresponding impedance module, Z_{NaCl}, in the y-axis was taken as the signal given by the NaCl solution. In a second step a diluted solution of BSA in 10^{-2} M NaCl was introduced and adsorption occurred over 600 s. After a short period of BSA incubation, a net increase of the impedance module was noted until reaching a plateau value, $Z_{NaCl,BSA}$, as displayed in Fig. 2. In the last step, the buffer was pumped again for 1100 s to ensure an efficient washing procedure. In order to have the same incubation time on the x-axis, all samples were introduced following the same procedure. The impedance module with time was normalised by the buffer response as the baseline because, as explained previously, we assume that the differential sensor response is directly related to the interfacial impedance which is itself linked to the interfacial capacitance. For that purpose, the obtained experimental plateau for the BSA adsorbed was defined as an equilibrium value: $\Delta Z_{BSA,eq} = Z_{NaCl,BSA} - Z_{NaCl}$. The maximum impedance module value obtained for $\Delta Z_{BSA,eq}$ for higher BSA concentration was taken as the experimental

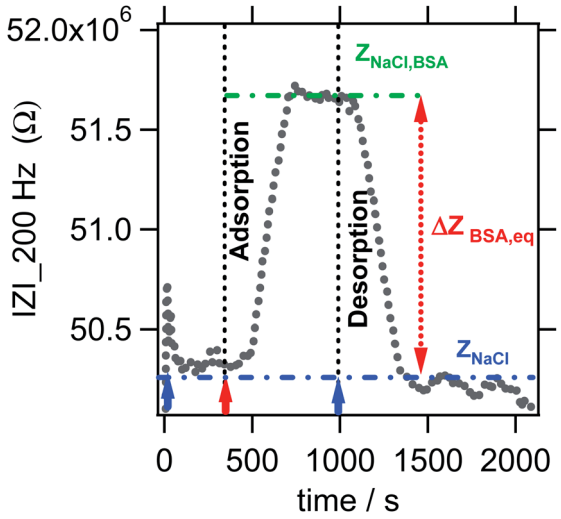

Fig. 2 Sensorgrams showing the impedance module with time for BSA adsorption and desorption steps onto the PET-microchannel at a fixed frequency and flow rate equal to 200 Hz and 7.2 μL min^{-1}, respectively. Step 1: the 10^{-2} M NaCl buffer was introduced for 360 s. Step 2: the diluted 5 pM BSA was introduced for 600 s for incubation. Step 3: the NaCl buffer was introduced again for the washing procedure for 1100 s.

plateau which corresponds to the theoretical maximum, $\Delta Z_{BSA,max}$. In the fitting procedure of the experimental data, the kinetic isotherm was normalized by $\Delta Z_{BSA,max}$ (see the right axis in Fig. 3A). Linearization of the adsorption isotherm was performed as illustrated in Fig. 3B.

Indeed, in the case of monolayer assumption, the biosensor response measured with time, $Z(t)$, increases proportionally with the surface concentration until the equilibrium is reached, while the quantity, $\Delta Z_{BSA,max} - Z(t)$, decreases proportionally with the adsorbed surface concentration maximum. In our case, the traditional Langmuir isotherm[19] adsorption does not fit well with the experimental data. We use the Langmuir–Freundlich combined equation[20,21] in order to approximate BSA adsorption onto the PET photoablated surface which can be viewed as an heterogeneous surface with different ionised groups generated on the PET surface by the photoablation process.[22]

Taking into account the Langmuir–Freundlich combined equation, the adsorbed surface concentration can be expressed as follows:

$$\frac{\Delta Z_{BSA,eq}}{\Delta Z_{BSA,max}} = \frac{KC^m}{1 + KC^m} = \frac{\Phi}{1 + \Phi} \quad (4)$$

where m exponent is the power term of the Freundlich isotherm and the parameter Φ can be viewed as the capacity of the system to reach the maximum coverage.

When $\Phi \ll 1$ (small coverage of the adsorbent, *i.e.* $\Delta Z_{BSA,eq} \ll \Delta Z_{BSA,max}$) this parameter can be neglected in the denominator of eqn (4).

Values of $K = 5 \times 10^4$ $M^{-0.43}$ and $m = 0.43$ were found after the fitting procedure with eqn (4) (see Fig. 3A) taking into account the measured experimental value of $\Delta Z_{BSA,max}$ equal to 4 MΩ.

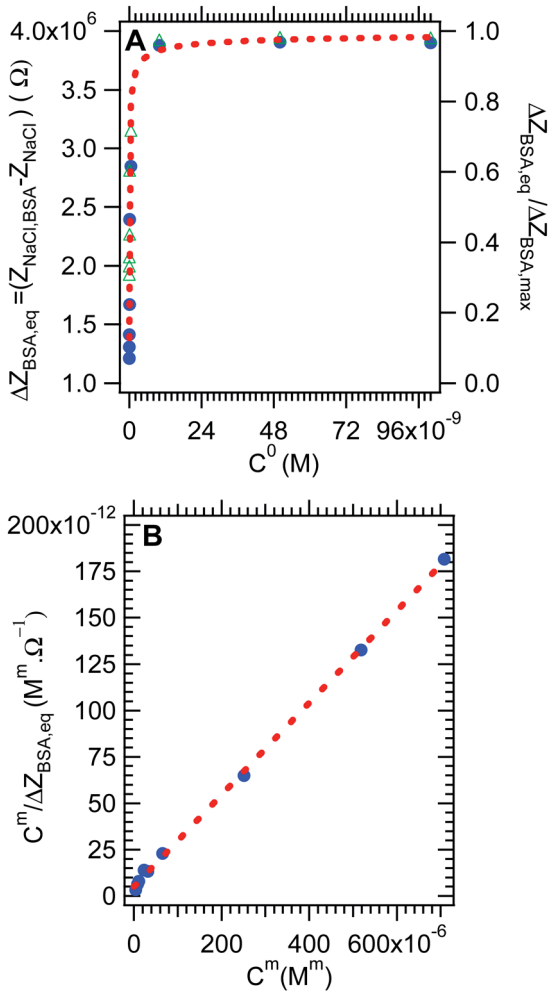

Fig. 3 Calibration for BSA detection on the PET-microchannel. (A) Isotherm of BSA adsorption obtained from the experimental sensorgrams at various concentrations from 1 pM to 100 nM (Fig. 2). The fit resulted in normalisation by experimental. Taking a value of $\Delta Z_{BSA,max} =$ 4 MΩ for normalization curves, values of $K = 5 \times 10^4$ $M^{-0.43}$ and $m =$ 0.43 were found after the fitting procedure with eqn (4). (B) Linearisation of the adsorption isotherm, following eqn (5): regression coefficient = 0.999, slope = 2.48×10^{-7} Ω^{-1}, intercept = 4.98×10^{-12} (M^m Ω^{-1}), from which $\Delta Z_{BSA,max} = 4.05$ M Ω and $K = 4.98 \times 10^4$ $M^{-0.43}$ were found.

A useful test traditionally used for Langmuir adsorption validation can be also extended to the Langmuir–Freundlich equation under a linear form as written in eqn (5) below:

$$\frac{C^m}{\Delta Z_{BSA,eq}} = \frac{1}{K \Delta Z_{BSA,max}} + \frac{C^m}{\Delta Z_{BSA,max}} \quad (5)$$

Linearisation using eqn (5) in Fig. 3B is in good agreement with the fit procedure and leads to $K = 4.98 \times 10^4$ $M^{-0.43}$ and $\Delta Z_{BSA,max} = 4.05$ MΩ.

The value of the K constant is in good agreement with those found in the literature. As an example, the experimental value obtained by James *et al.*[20] for BSA adsorbed in anion exchanger (DEAE-Sepharose Fast Flow) medium at pH 9 and 0.012 M NaCl was equal to $K = 6.64$ 10^4 $M^{-0.86}$. This confirms our choice using the power law equation for the adsorption fit procedure which is generally applied for the heterogeneous surface. In this device, the semi-crystalline surface of the photoablated PET can act as a heterogeneous surface due to the different functional groups existing on its surface, even after the photoablation process.[22]

3.3 Methodology for interfacial impedance in the microchannel

In the microchannel, the impedance is represented by an $R_S//C_S$ circuit. The resistance, R_S, is characteristic of the electrolyte resistance and C_S is the cell capacitance. This capacitance is observed at very high frequencies mainly in dielectric media.

The study of the dielectrical response of the microchip shows that at low frequencies, the impedance contribution (Z_2) of the PET thickness (120 μm) between the microelectrodes can be neglected. The correction of the global impedance (Z_G) performed in previous work[15] is not necessary, which indicates that at 200 Hz the global impedance (Z_G) is assimilated to the impedance measured through the microchannel (Z_1).

The contribution of the interfacial impedance can be expressed as follows:

$$\frac{1}{(j\omega)^{\alpha_{int}} Q_{int}} = \frac{\cos\left(-\frac{\pi\alpha_{int}}{2}\right) + j \sin\left(-\frac{\pi\alpha_{int}}{2}\right)}{\omega^{\alpha_{int}} Q_{int}} \quad (6)$$

The expression of the impedance Z_1 can be further written as:

$$Z_1(\omega) = \frac{(1 + j\omega R_S(C_S + C_{PET,1}))(-\omega^2 C_{PET,1} R_S C_S - j\omega C_{PET,1})}{(-\omega^2 C_{PET,1} R_S C_S)^2 + (\omega C_{PET,1})^2} + \frac{\cos\left(\frac{\pi\alpha_{int}}{2}\right) + j \sin\left(-\frac{\pi\alpha_{int}}{2}\right)}{\omega^{\alpha_{int}} Q_{int}} \quad (7)$$

After development, we obtain the following expression of the impedance Z_1 where one can clearly identify the real part, $\mathrm{Re}(Z_1(\omega))$, and the imaginary part, $\mathrm{Im}(Z_1(\omega))$.

$$Z_1(\omega) = \frac{\left(\omega^2 {C_{PET,1}}^2 R_S\right)}{(\omega^2 C_{PET,1} R_S C_S)^2 + (\omega C_{PET,1})^2} + \frac{\cos\left(\frac{\pi\alpha_{int}}{2}\right)}{\omega^{\alpha_{int}} Q_{int}} + j\left[\frac{\sin\left(-\frac{\pi\alpha_{int}}{2}\right)}{\omega^{\alpha_{int}} Q_{int}} - \frac{(\omega^3 C_{PET,1} {R_S}^2 C_S (C_S + C_{PET,1}) + \omega C_{PET,1})}{(\omega^2 C_{PET,1} R_S C_S)^2 + (\omega C_{PET,1})^2}\right] \quad (8)$$

with

$$\mathrm{Re}[Z_1(\omega)] = \frac{\left(\omega^2 {C_{PET,1}}^2 R_S\right)}{(\omega^2 C_{PET,1} R_S C_S)^2 + (\omega C_{PET,1})^2} + \frac{\cos\left(\frac{\pi\alpha_{int}}{2}\right)}{\omega^{\alpha_{int}} Q_{int}} \quad (9)$$

and

$$\mathrm{Im}[Z_1(\omega)] = -\left[\frac{\sin\left(-\frac{\pi\alpha_{int}}{2}\right)}{\omega^{\alpha_{int}} Q_{int}} + \frac{(\omega^3 C_{PET,1} {R_S}^2 C_S (C_S + C_{PET,1}) + \omega C_{PET,1})}{(\omega^2 C_{PET,1} R_S C_S)^2 + (\omega C_{PET,1})^2}\right] \quad (10)$$

Wherein the target application is the real-time monitoring of the interfacial impedance in the microchannel, the imaginary part only of the impedance which contains the contribution of the interfacial is taken into account at 200 Hz.

Finally the interfacial impedance is defined as follows:

$$Q_{\text{int}} = \frac{\sin\left(\frac{\pi\alpha_{\text{int}}}{2}\right)}{(\omega)^{\alpha_{\text{int}}}\left[-\text{Im}[Z_1(\omega)] - \frac{(\omega^2 {R_S}^2 C_S(C_S + C_{\text{PET},1}) + 1)}{(\omega^3 C_{\text{PET},1})(C_S R_S)^2 + (\omega C_{\text{PET},1})}\right]} \quad (11)$$

It will be more convenient to have an expression, as presented by eqn (11), which gives a quick estimation of free contact microchannel interfacial impedance from a read value of the imaginary part of impedance at a fixed low frequency. By recording the imaginary part variation against time at a given frequency, it will be possible to deduce the interfacial impedance Q_{int} in the microchannel using the previous equation.

The numerical values of C_S, R_S, $C_{\text{PET},1}$, and α_{int} were considered as being fixed and obtained in previous studies by fitting of the Nyquist plot.[16] We obtained the same parameter values in this study: $C_S = 2 \times 10^{-13}$ F, $R_S = 3.5 \times 10^7$ Ω, $C_{\text{PET},1} = 14 \times 10^{-11}$ F, and $\alpha_{\text{int}} = 0.5$.

This can finally lead to an analytical expression for the interfacial impedance from the realtime monitoring of the experimental imaginary values of the impedance Z_1 at a fixed frequency in time.

By replacing the parameter values of C_S, R_S, $C_{\text{PET},1}$, and α_{int} in eqn (11) at $f = 200$ (Hz) we obtained the following analytical equation for Q_{int}:

$$Q_{\text{int}} = \frac{0.707}{35.44[-\text{Im}[Z_1(\omega)] - 6 \times 10^6]} \quad (12)$$

From this equation, at the selected frequency of 200 Hz, the value of 6×10^6 in the denominator is negligible compared to the values of the imaginary part which are on the order of 6×10^8. As a consequence, the impedance measurement at a fixed frequency can be exploited to calculate the values of the interfacial impedance, which is related to the adsorbed BSA concentration. The plot of Q_{int} according to the BSA concentration at 1 pM is illustrated in Fig. 4. By following the same procedure described above, Q_{int} change with time is normalised with the buffer response as the baseline.

The obtained experimental plateau for the BSA adsorbed was defined as an equilibrium value: $\Delta Q_{\text{int,BSA,eq}} = Q_{\text{int,NaCl}} - Q_{\text{int,-NaCl,BSA}}$. Theoretically, the maximum of the value $\Delta Q_{\text{int,BSA,max}}$ must be obtained for higher BSA concentration. However, the application of eqn (12) for concentrations above 100 pM does not permit obtaining consistent values. The plot $\Delta Q_{\text{int,BSA,eq}}$ estimated for low BSA concentrations (1 pM to 100 pM) is presented in Fig. 5. A linear variation between the BSA concentration in the microchannel and the value of the interfacial impedance is obtained only for ultralow concentrations. This representation can be used as a calibration curve in the following concentration range: from 1 pM to 100 pM.

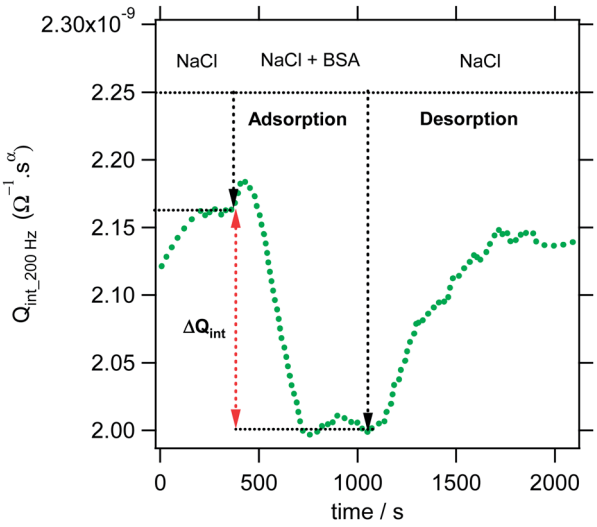

Fig. 4 Sensorgrams showing Q_{int} change calculated using eqn (12) with time for BSA adsorption and desorption steps at 200 Hz and a flow rate equal to 7.2 μL min^{-1}. Step 1: the 10^{-2} M NaCl buffer was introduced for 360 s. Step 2: the diluted 1 pM BSA was introduced for 600 s for incubation. Step 3: the NaCl buffer was introduced again for the washing procedure for 1100 s.

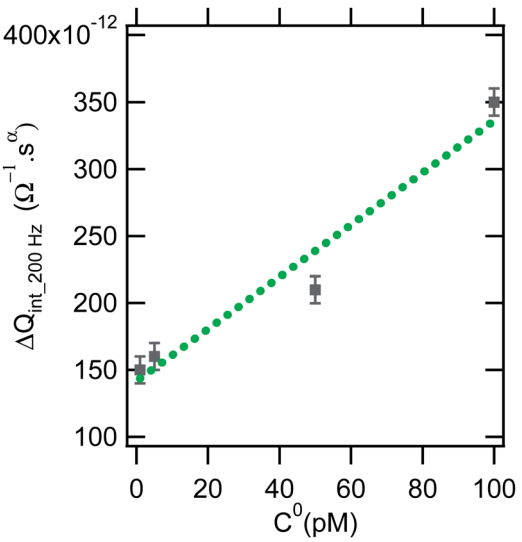

Fig. 5 Calibration curve of the normalised $\Delta Q_{\text{int,BSA,eq}}$ *versus* BSA concentration for ultralow concentrations from 1 pM to 100 pM at a fixed frequency of 200 Hz.

4 Conclusions

Previous articles have demonstrated the feasibility of temporal monitoring of adsorption and desorption of lactoglobulin on PET coated with gold nanoparticles[14] or antibodies on gold nanowires as carpets on a hybrid polycarbonate membrane.[23] However, this present study with the associated model underlines a direct procedure to monitor adsorption kinetics and detect ultralow concentrations of adsorbed protein on photo-ablated PET without modification such as coating with gold nano-objects. The experimental results show very good

reproducibility with negligible variation of the signal. As portrayed in Fig. 5, the threshold of detection is close to the picomolar concentration. As expected, due to the tunability of the surface charge, the interfacial impedance increases with the BSA concentration. The main process governing the electrical properties of the sensor is the adsorption of charged BSA onto the photoablated PET surface. Indeed, BSA contains several amino acid functional groups in side chains, which are either positively or negatively charged. For example, Arg, His, and Lys are positively charged and Asp, Glu, Tyr, and Cys are negatively charged. These groups are in different proportions in the BSA. At pH 9, BSA is known to be negatively charged[24] and we suppose that its adsorption on the photoablated PET surface causes a change of the charged region in the Gouy–Chapman layer. The work in progress concerns the realtime monitoring of biomolecular recognition of BSA adsorbed on PET by using the corresponding rabbit anti-BSA antibodies as analytes in the flow microchannel.

Notes and references

1 J. Lichtenberg, N. F. de Rooij and E. Verpoorte, *Electrophoresis*, 2002, **23**, 3769–3780.
2 J. Gamby, M. Lazerges, C. Pernelle, H. Perrot, H. H. Girault and B. Tribollet, *Lab Chip*, 2007, **7**, 1607–1609.
3 D. Figeys and D. Pinto, *Electrophoresis*, 2001, **22**, 208–216.
4 R. Schirhagl, U. Latif, D. Podlipna, H. Blumenstock and F. L. Dickert, *Anal. Chem.*, 2012, **84**, 3908–3913.
5 S. Qi, X. Liu, S. Ford, J. Barrows, G. Thomas, K. Kelly, A. McCandless, K. Lian, J. Goettert and S. A. Soper, *Lab Chip*, 2002, **2**, 88–95.
6 J. R. Epstein, I. Biran and D. R. Walt, *Anal. Chim. Acta*, 2002, **469**, 3–36.
7 A. Gaspar and F. A. Gomez, *Electrophoresis*, 2012, **33**, 1723–1728.
8 P. Schuck, L. F. Boyd and P. S. Andersen in *Measuring Protein Interactions by Optical Biosensors*, John Wiley & Sons, Inc., 2001.
9 H. J. Lee, T. T. Goodrich and R. M. Corn, *Anal. Chem.*, 2001, **73**, 5525–5531.
10 Y. Zhang, M. Xu, M. Du and F. Zhou, *Electrophoresis*, 2007, **28**, 1839–1845.
11 F. H. Arnold, H. W. Blanch and C. R. Wilke, *Chem. Eng. J.*, 1985, **30**, B9–B23.
12 H. Kitano, K. Nakamura, Y. Hirai, T. Kaku and N. Ise, *Biotechnol. Bioeng.*, 1988, **31**, 547–552.
13 R. L. Wimalasena and G. S. Wilson, *J. Chromatogr.*, 1991, **572**, 85–102.
14 J. Gamby, J. P. Abid, B. Tribollet and H. H. Girault, *Small*, 2008, **4**, 802–809.
15 M. Faure, M. Kechadi, B. Sotta, J. Gamby and B. Tribollet, *Electroanalysis*, 2013, **25**, 1151–1158.
16 M. Kechadi, J. Gamby, L. Chaal, H. Girault, B. Saidani and B. Tribollet, *Electrochim. Acta*, 2013, **105**, 7–14.
17 J. Gamby, J.-P. Abid and H. H. Girault, *J. Am. Chem. Soc.*, 2005, **127**, 13300–13304.
18 M. Kechadi, J. Gamby, L. Chaal, B. Saidani and B. Tribollet, *J. Flow Chem.*, 2013, **3**, 81–86.
19 I. Langmuir, *J. Am. Chem. Soc.*, 1918, **40**, 1361–1403.
20 E. A. James and D. D. Do, *J. Chromatogr.*, 1991, **542**, 19–28.
21 G. P. Jeppu and T. P. Clement, *J. Contam. Hydrol.*, 2012, **129–130**, 46–53.
22 F. Bianchi, Y. Chevolot, H. J. Mathieu and H. H. Girault, *Anal. Chem.*, 2001, **73**, 3845–3853.
23 J. Gamby, J. P. Abid, M. Abid, J. P. Ansermet and H. H. Girault, *Anal. Chem.*, 2006, **78**, 5289–5295.
24 K. Rezwan, L. P. Meier and L. J. Gauckler, *Langmuir*, 2005, **21**, 3493–3497.